IOP Publishing New J. Phys. 25 (2023) 073009 https://doi.org/10.1088/1367-2630/ace3eb

New Journal of Physics
The open access journal at the forefront of physics

Deutsche Physikalische Gesellschaft DPG
IOP Institute of Physics

Published in partnership with: Deutsche Physikalische Gesellschaft and the Institute of Physics

OPEN ACCESS

RECEIVED
9 October 2022

REVISED
20 June 2023

ACCEPTED FOR PUBLICATION
4 July 2023

PUBLISHED
17 July 2023

PAPER

Nonreciprocal single-photon state conversion between microwave and optical modes in a hybrid magnonic system

Jikun Xie[1], **Shengli Ma**[1,*], **Yalong Ren**[1], **Xinke Li**[2,*], **Shaoyan Gao**[1] **and Fuli Li**[1,*]

[1] MOE Key Laboratory for Non-equilibrium Synthesis and Modulation of Condensed Matter, Shaanxi Province Key Laboratory of Quantum Information and Quantum Optoelectronic Devices, School of Physics, Xi'an Jiaotong University, Xi'an 710049, People's Republic of China

[2] School of Mathematics, Physics and Optoelectronic Engineering, Hubei University of Automotive Technology, Shiyan 442002, People's Republic of China

[*] Authors to whom any correspondence should be addressed.

E-mail: msl1987@xjtu.edu.cn, 20210064@huat.edu.cn and flli@xjtu.edu.cn

Keywords: quantum magnonics, microwave-optical conversion, nonreciprocal single-photon transmission, quantum networks

Abstract

Coherent quantum transduction between microwave and optical signals is of great importance for long-distance quantum communication. Here we propose a novel scheme for the implementation of nonreciprocal single-photon state conversion between microwave and optical modes based on a hybrid magnonic system. A yttrium–iron–garnet (YIG) sphere with both the optomechanical and the optomagnetic properties is exploited to couple with a three-dimensional superconducting microwave resonator. The magnetostatic mode of the YIG sphere is treated as an intermediate to interact with the microwave and optical modes simultaneously. By manipulating the amplitudes and phase differences between the couplings via external driving fields, we show that the nonreciprocal microwave-light single-photon state conversion can be realized via the quantum interference effect.

1. Introduction

Hybrid quantum systems have been extensively studied to harness the advantages of distinct physical systems for implementing various kinds of quantum information protocols [1–3]. The crucial requirement on this subject is to achieve the strong coupling between different physical subsystems [3–5]. Recently, the ferromagnetic crystal [6–8], especially the yttrium–iron–garnet (YIG) coupled to superconducting microwave cavity has received great attention as an alternative approach to realize strong light–matter interactions [9–13].

YIG is a representative ferrite material with excellent dielectric properties and high Curie temperature. Thanks to its high spin density and low damping rate, the strong and even ultrastrong coupling between magnons (the quanta of collective spin excitations) and microwave photons have already been observed [14–22]. Experimentally, significant progress has been made based on this hybrid cavity magnonic system for many quantum technological applications [23–39]. In addition, the magnetic excitations in the YIG sphere can lead to the geometric deformation of the surface. Thus, the magnetic modes can also couple to the mechanical modes through magnetostrictive interactions [40, 41]. In the light of these advances, a series of theoretical works have been proposed for realizing quantum entanglement [42–50], non-Hermitian effects [51–55], phonon laser [56, 57], magnon blockade [58–62], nonreciprocity [63–66], etc.

On the other hand, the YIG sphere itself can also be shaped into an optical whispering gallery mode (WGM) cavity with high quality factor and relatively small mode volume [67–70]. When the triple-resonance condition is satisfied, the optical WGMs can couple to magnon modes by means of the Brillouin scattering process [71–74]; that is, the input and output optical modes are resonant with the frequency difference given by a magnon mode [75]. The triple resonance can be readily achieved by tuning

the magnon frequency via the external bias magnetic field. This emerging field of cavity optomagnonics has received considerable attentions [76–89]. Since the magnon modes can couple to both the microwave and optical photons, it is therefore desirable to exploit the YIG sphere to realize a microwave-to-optical transducer [90, 91]. Moreover, recent experiments have reported the bidirectional conversion between the microwave and optical modes via a ferromagnetic mode [92–94].

In this paper, we takes a step forward, i.e. the nonreciprocal microwave-optical single-photon state conversion is studied in a hybrid quantum magnonic system. The proposed setup is based on a YIG sphere with both optomechanical and optomagnetic properties coupled to a three-dimensional microwave cavity. The YIG sphere itself holds the magnon, optical and mechanical modes simultaneously, and these three modes couple to each other through the magnetostrictive, optomagnonic and optomechanical interactions, respectively. By turning the external driving fields, the magnitude ratios and phase differences of those couplings can be controlled. As a result, breaking of time-reversal symmetry can be achieved, leading to the desired the optical nonreciprocity. We show that the designed optical component enables a high-performance nonreciprocal single-photon state conversion between the microwave and optical modes through the quantum interference of two possible paths. The conversion of photons from one frequency to the other one is enhanced by the constructive quantum interference, while the conversion in the reversal direction is suppressed due to the destructive quantum interference. Moreover, the optical nonreciprocity can also be reversed on-demand by changing the phase differences. The interface [95–101] and the nonreciprocal single-photon conversion [102–107] between microwave and optical modes is of great importance in noise-tolerant quantum networks. So, our work may stimulate many practical quantum applications based on the hybrid ferromagnetic system.

2. Model and Hamiltonian

As schematically depicted in figure 1, we investigate a hybrid quantum system of a YIG sphere with both the optomechanical and optomagnetic properties coupled to a three-dimensional microwave cavity through magnetic dipole interaction [15, 16]. The YIG sphere is placed at the antinode of microwave magnetic field in the three-dimensional microwave cavity and locally biased with a static magnetic field **H**. It is well known that many magnetostatic modes can be excited in the YIG sphere, when the magnetic component of the microwave cavity field is perpendicular to the bias magnetic field. Here, we only focus on the simplest magnetostatic mode, i.e. the Kittel mode [108] that has the uniform spin precessions in the whole volume of YIG sphere and the highest magnetic coupling strength with the microwave cavity [93]. Additionally, the YIG itself is shaped into a whispering gallery resonator that supports optical WGMs. The Kittel mode can interact with the optical transverse electric (TE) mode and transverse magnetic (TM) mode through a three-wave process, i.e. a Brillouin light scattering process [71, 72]. Owing to the deformation of the geometry structure, we also consider an intrinsic vibrational mode of the YIG sphere, and the associated phonons are coupled to the optical photons via the radiation pressure and to the magnons via the magnetostrictive interaction [40, 41]. Thus, the free Hamiltonian of the whole system reads ($\hbar = 1$ hereafter)

$$H_0 = \sum_{\beta} \omega_\beta \beta^\dagger \beta, \tag{1}$$

where ω_β is the resonance frequency, and β and $\beta^\dagger$ are the annihilation and creation operators ($\beta = a, b, c, m, r$ represents the TM, TE, microwave cavity, magnon and phonon modes, respectively).

Furthermore, the interactions between different modes can be described by the following Hamiltonian

$$\begin{aligned} H_I = {} & g_m \left(ab^\dagger + a^\dagger b\right)\left(m^\dagger + m\right) + G_{mc}\left(c^\dagger + c\right)\left(m^\dagger + m\right) \\ & + g_{mr} m^\dagger m \left(r^\dagger + r\right) + g_{br} b^\dagger b \left(r^\dagger + r\right). \end{aligned} \tag{2}$$

In the above equation, g_m is the single-photon Brillouin coupling rate, G_{mc} represents the coupling strength between the magnon and microwave photon, g_{mr} denotes the single-magnon magnomechanical coupling rate and g_{br} describes the single-photon optomechanical coupling strength between the TE and the phonon mode. Because the vibration direction of the mechanical mode and the field direction of the TM mode is orthogonal [80], there is no direct coupling between the mechanical mode and the TM mode. To enhance and linearize the optomagnonic, magnomechanical as well as the optomechanical interactions, we drive the TM, TE and magnon modes simultaneously. The Hamiltonian that describes coherent driving is given by

$$H_d = \left(\Omega_a a^\dagger e^{-i(\omega_{da} t + \theta_a)} + \Omega_b b^\dagger e^{-i(\omega_{db} t + \theta_b)} + \Omega_m m^\dagger e^{-i(\omega_{dm} t + \theta_m)} + H.c.\right), \tag{3}$$

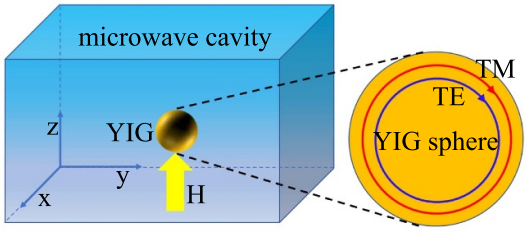

Figure 1. Schematic diagram of the hybrid quantum system. A YIG sphere is placed inside a three-dimensional microwave cavity near the maximum magnetic field of the cavity mode, and simultaneously biased by a uniform static magnetic field **H**, enabling a strong coupling between magnons and microwave photons. The magnon mode is directly driven by a microwave source to enhance the magnomechanical coupling. In addition, the TE and TM mode of the YIG microsphere cavity is coupled to the magnon mode through a Brillouin light scattering process.

where $\Omega_a = \sqrt{2\kappa_a P_a/\omega_{da}}$ ($\Omega_b = \sqrt{2\kappa_b P_b/\omega_{db}}$) denotes the coupling between the TM (TE) mode and the external laser field with phase θ_a (θ_b), κ_a (κ_b) is the external coupling rates, P_a (P_b) is the driving power, and ω_{da} (ω_{db}) represents the oscillating frequency of the driving field to the TM (TE) mode. In addition, the Rabi frequency $\Omega_m = \frac{\sqrt{5}}{4}\gamma\sqrt{N}B_0$ describes the coupling of the applied AC magnetic field (with amplitude B_0, driving frequency ω_{dm} and phase θ_m) to the Kittel mode, where $\gamma/2\pi = 28$ GHz T^{-1} is the gyromagnetic ratio, and $N = \rho V_m$ is the total number of spins, i.e. V_m is the volume and $\rho = 4.22 \times 10^{27}$ m^{-3} is the spin density of the YIG sphere.

Now, we apply a unitary transformation $U_1(t) = e^{-iH_0' t}$ with $H_0' = \omega_{da} a^\dagger a + \omega_{db} b^\dagger b + \omega_{dm}(m^\dagger m + c^\dagger c)$. Then, the total Hamiltonian yields

$$\begin{aligned} H_t = &\sum_\alpha \Delta_\alpha' \alpha^\dagger \alpha + \omega_r r^\dagger r + \left[g_m a b^\dagger e^{-i(\omega_{da}-\omega_{db})t}\left(m^\dagger e^{i\omega_{dm}t} + m e^{-i\omega_{dm}t}\right)\right. \\ &+ \left(g_{br} b^\dagger b + g_{mr} m^\dagger m\right) r + G_{mc} c^\dagger e^{i\omega_{dm}t}\left(m^\dagger e^{i\omega_{dm}t} + m e^{-i\omega_{dm}t}\right) \\ &\left. + H.c.\right] + \left(\Omega_a e^{-i\theta_a} a^\dagger + \Omega_b e^{-i\theta_b} b^\dagger + \Omega_m e^{-i\theta_m} m^\dagger + H.c.\right) \end{aligned} \tag{4}$$

with $\alpha = a, b, c, m$, $\Delta_a' = \omega_a - \omega_{da}$, $\Delta_b' = \omega_b - \omega_{db}$, $\Delta_c' = \omega_c - \omega_{dm}$ and $\Delta_m' = \omega_m - \omega_{dm}$. Provided that the two conditions $\omega_{db} - \omega_{da} - \omega_{dm} = 0$ and $\omega_{dm} \gg G_{mc}, g_m$ are satisfied, we can safely neglect those fast oscillating terms in equation (4) under the rotating-wave approximation. After that, the total Hamiltonian of the whole system will reduce to the form

$$\begin{aligned} H_t = &\sum_\alpha \Delta_\alpha' \alpha^\dagger \alpha + \omega_r r^\dagger r + [g_m a b^\dagger m + G_{mc} c^\dagger m + (g_{br} b^\dagger b + g_{mr} m^\dagger m) r \\ &+ H.c.] + (\Omega_a e^{-i\theta_a} a^\dagger + \Omega_b e^{-i\theta_b} b^\dagger + \Omega_m e^{-i\theta_m} m^\dagger + H.c.). \end{aligned} \tag{5}$$

After a standard linearization procedure under the strong driving conditions, we can obtain the linearized Hamiltonian

$$\begin{aligned} H_{\rm lin} = &\sum_\alpha \Delta_\alpha \alpha^\dagger \alpha + \omega_r r^\dagger r + \left[G_{ab} a b^\dagger + G_{am} a^\dagger m^\dagger + G_{mc} m c^\dagger \right. \\ &\left. + G_{mb} m b^\dagger + \left(G_{br} b^\dagger + G_{mr} m\right)\left(r^\dagger + r\right) + H.c.\right] \end{aligned} \tag{6}$$

with $\Delta_{a,c} = \Delta_{a,c}'$, $\Delta_b = \Delta_b' + g_{br}(r_s^* + r_s)$ and $\Delta_m = \Delta_m' + g_{mr}(r_s^* + r_s)$. In equation (6), $G_{am} = g_m b_s$, $G_{ab} = g_m m_s$, $G_{mb} = g_m a_s$, $G_{br} = g_{br} b_s$ and $G_{mr} = g_{mr} m_s^*$ describe the effective field-enhanced coupling strengths. Here, a_s, b_s, c_s, m_s and r_s are the steady state classical mean values of the a, b, c, m and r modes, respectively. Details of the derivations of the above Hamiltonian are given in appendix.

To go a further step, we perform another unitary transformation $U_2(t) = e^{-iH_0'' t}$ to equation (6) with $H_0'' = \sum_\alpha \Delta_\alpha \alpha^\dagger \alpha + \omega_r r^\dagger r$. If the parameters are chosen to be $\Delta_b = \Delta_c = \Delta_m = \omega_r \gg \{G_{mb}, G_{mc}, G_{mr}, G_{br}\}$, $\Delta_a + \Delta_m \gg G_{am}$ and $\Delta_a - \Delta_b \gg G_{ab}$, we can use the rotating-wave approximation to neglect those fast oscillating terms; that is, the TM mode can be safely eliminated. Then, the associated interaction Hamiltonian can be written as

$$H = G_{mc} m c^\dagger + G_{mb} m b^\dagger + G_{mr} m r^\dagger + G_{br} b^\dagger r + H.c.. \tag{7}$$

As depicted in figure 2, the effective couplings of this hybrid quantum system is revealed. Notably, both the magnitude and phase of the couplings can be well controlled by changing the external driving fields [103].

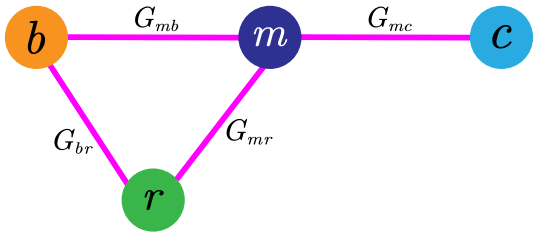

Figure 2. The effective interaction of the hybrid quantum system. The magnon mode as a mediator is used to couple to both the microwave mode and TE mode. Besides, an auxiliary phonon mode interacts with both the magnon mode and TE mode, and a coupling loop is formed.

Without loss of generality, we assume that the coupling constants G_{mb} and G_{br} are positive real numbers, and $G_{mr} = |G_{mr}|e^{i\phi}$ is a complex number with a nontrivial phase ϕ. In such a circumstance, the existence of the nontrivial phase ϕ is related to an artificial synthetic magnetism penetrating the closed-loop [109–112], which is formed by the couplings G_{mb}, G_{mr} and G_{br}. As a result, the time-reversal symmetry is broken, and we can realize a nonreciprocal quantum transduction between the microwave and optical signals.

3. Nonreciprocal single-photon state conversion

In this section, we discuss in detail how to realize the nonreciprocal microwave-light single-photon state conversion based on the above mentioned hybrid quantum system, which is an important step towards the long-distance quantum communication. To obtain this goal, we need to investigate the quantum dynamics of our system by solving the quantum Langevin equations (QLEs). To this end, we define vectors $v = [c, m, b, r]^T$ of annihilation operators and $v_{\rm in} = [c_{\rm in}, m_{\rm in}, b_{\rm in}, r_{\rm in}]^T$ with respect to noise operators. Here, these sources of noise obey the following correlation relations

$$\begin{aligned}
&\left\langle c_{\rm in}^{\dagger}(t)c_{\rm in}(t')\right\rangle = n_{c,\rm th}\delta(t-t'),\ \left\langle m_{\rm in}^{\dagger}(t)m_{\rm in}(t')\right\rangle = n_{m,\rm th}\delta(t-t'),\\
&\left\langle b_{\rm in}^{\dagger}(t)b_{\rm in}(t')\right\rangle = n_{b,\rm th}\delta(t-t'),\ \left\langle r_{\rm in}^{\dagger}(t)r_{\rm in}(t')\right\rangle = n_{\rm th}\delta(t-t'),
\end{aligned} \tag{8}$$

where $n_{\alpha,\rm th} = 1/(e^{\hbar\omega_\alpha/k_{\rm B}T}-1)$ $(\alpha = c, m, b)$ and $n_{\rm th} = 1/(e^{\hbar\omega_r/k_{\rm B}T}-1)$ are the thermal occupations with the environmental temperature T and the Boltzmann constant $k_{\rm B}$. To effectively suppress these thermal excitations, we consider the experimental working temperature $T = 10$ mK. In this situation, the thermal phonon number is about $n_{\rm th} = 1.69$ for the mechanical frequency $\omega_r/2\pi = 100$ MHz. Additionally, the optical, microwave, and magnon modes have a relative large resonance frequency, whose thermal occupations are negligible. Hence, we neglect the thermal excitations of the optical, microwave, and magnon modes in the following discussions.

According to the Heisenberg equations of motion and together with the corresponding damping and noise terms, we can derive the QLE of the vector v as

$$i\frac{{\rm d}v}{{\rm d}t} = Mv + i\sqrt{K}v_{\rm in} \tag{9}$$

with the coefficient matrix

$$M = \begin{pmatrix} -i\kappa_c/2 & G_{mc} & 0 & 0 \\ G_{mc} & -i\kappa_m/2 & G_{mb} & G_{mr}^{*} \\ 0 & G_{mb} & -i\kappa_b/2 & G_{br} \\ 0 & G_{mr} & G_{br} & -i\kappa_r/2 \end{pmatrix} \tag{10}$$

and the diagonal matrix $\sqrt{K} = {\rm Diag}\left[\sqrt{\kappa_c}, \sqrt{\kappa_m}, \sqrt{\kappa_b}, \sqrt{\kappa_r}\right]$. Here, κ_b and κ_c are the external coupling rates, and we have neglected the internal decay rates of the TE and microwave modes in our scheme. There are no external input signals for the mechanical and magnetic modes. So, κ_r and κ_m can be regarded as their total damping rates. Since the time evolution only involves the beam-splitter interactions, our system is always stable for arbitrary parameters. By introducing the Fourier transformation $o(t) = \int {\rm d}\omega e^{-i\omega t}o(\omega)/2\pi$ for an operator o, we proceed to convert equation (9) into the frequency domain

$$v(\omega) = i(\omega I - M)^{-1}\sqrt{K}v_{\rm in}(\omega), \tag{11}$$

where I represents the 4×4 identity matrix. To achieve the output fields, we further define the output operators $v_{\rm out} = [c_{\rm out}, m_{\rm out}, b_{\rm out}, r_{\rm out}]^T$. By substituting equation (11) into the standard input–output theorem $v_{\rm out}(\omega) = v_{\rm in}(\omega) - \sqrt{K}v(\omega)$, we can figure out the formula $v_{\rm out} = T(\omega)v_{\rm in}$, where

$$T(\omega) = I - i\sqrt{K}(\omega I - M)^{-1}\sqrt{K} \tag{12}$$

is a unitary matrix. Here, the matrix element $T_{ij}(\omega)$ describes the transmission amplitude from the mode j to the mode i ($i,j = 1,2,3,4$ is referred to c, m, b, r, respectively). In the absence of thermal phonon noise, $T(\omega)$ characterizes the transmission probability from the input single-photon state to the output one [113]. To well illustrate the mechanism of nonreciprocal quantum transduction, we start our discussion by neglecting the thermal phonon noise, whose effect will be discussed in the next section.

First of all, we consider the situation that an input single-photon is in resonance with the cavity frequency, i.e. $\omega = 0$. The nonreciprocal conversion of the single-photon state with a finite bandwidth will be later analyzed. To realize a perfect one-way quantum transduction from the microwave mode c to the optical mode b, we must guarantee that the transmission matrix elements satisfy $T_{13}(0) = 0$ and $T_{31}(0) = 1$. According to equation (12), we can derive out the ratio of the transmission matrix element $T_{13}(0)$ to $T_{31}(0)$; that is

$$\frac{T_{13}(0)}{T_{31}(0)} = \frac{G_{mb} - 2iG_{br}|G_{mr}|e^{-i\phi}/\kappa_r}{G_{mb} - 2iG_{br}|G_{mr}|e^{i\phi}/\kappa_r}. \tag{13}$$

Particularly, if the parameters are chosen to be $|G_{mr}| = G_{mb}\kappa_r/2G_{br}$ and $\phi = \pi/2$, we have $T_{13}(0) = 0$ and $T_{31}(0) \neq 0$. This is the obvious nonreciprocal conditions, under which the input quantum signal of microwave mode c can be converted to the output one of the optical mode b, but not vice versa. Physically, this nonreciprocity originates from the artificial synthetic magnetism. As seen in figures 3(a) and (b), the phase difference ϕ among couplings G_{mb}, G_{mr} and G_{br} is equivalent to creating a synthetic magnetic flux threading the closed loop. When $\phi \neq n\pi$ is satisfied (n is an integer), the time-reversal symmetry is broken, leading to the desired optical nonreciprocity. For the specifical magnetic flux of $\phi = \pi/2$, the three modes m, b and r play the role of a three-port circulator; that is, it allows for the quantum signal transmission along the counterclockwise direction due to the quantum interference effect ($m \to b \to r \to m$) [114, 115]. As shown in figure 3(a), the input single-photon state of microwave cavity c can be transferred to the output of optical cavity b along two possible paths, where one path is along $c \to m \to b$ and the other one is along $c \to m \to r \to b$. Under the nonreciprocal conditions, the constructive interference occurs between the two paths, which results in the enhancement of the matrix element $T_{31}(0)$. On the contrary, as displayed in figure 3(b), the transmission from the mode b to c is completely suppressed due to the destructive interference between the two paths ($b \to m \to c$ and $b \to r \to m \to c$). This is the mechanism for the realization of nonreciprocal quantum transduction.

Besides, it is also noteworthy here that the optical nonreciprocity can be reversed if the relative phase is switched to $\phi = -\pi/2$. Then, we can acquire an unidirectional single-photon state conversion from the optical to microwave fields, i.e. $T_{13}(0) \neq 0$ and $T_{31}(0) = 0$. To simplify our discussion, we only concentrate on the situation of $\phi = \pi/2$, i.e. the one-way quantum conversion from the microwave to optical photons.

As discussed above, $T_{13}(0) = 0$ can be achieved in terms of the nonreciprocal conditions $|G_{mr}| = G_{mb}\kappa_r/2G_{br}$ and $\phi = \pi/2$. However, to ensure an ideal nonreciprocal optical component, the condition $T_{31}(0) = 1$ should be met at the same time. Consequently, it also requires $|T_{i1}(0)/T_{31}(0)| \ll 1$ ($i = 2,4$), which can prevent the loss of input photons to other modes. By setting $G_{br} = \sqrt{\kappa_b\kappa_r}/2$, we can deduce $T_{41}(0) = 0$ from the equation (12), indicating that the transmission from the microwave mode to mechanical mode is totally inhibited. We now can give the full transmission matrix on resonance (i.e. $\omega = 0$)

$$T(0) = \begin{pmatrix} -\frac{\kappa_m+\Gamma_b-\Gamma_c}{\kappa_m+\Gamma_b+\Gamma_c} & \frac{2i\sqrt{\kappa_m\Gamma_c}}{\kappa_m+\Gamma_b+\Gamma_c} & 0 & -\frac{2i\sqrt{\Gamma_b\Gamma_c}}{\kappa_m+\Gamma_b+\Gamma_c} \\ \frac{2i\sqrt{\kappa_m\Gamma_c}}{\kappa_m+\Gamma_b+\Gamma_c} & \frac{\Gamma_b+\Gamma_c-\kappa_m}{\kappa_m+\Gamma_b+\Gamma_c} & 0 & \frac{2\sqrt{\kappa_m\Gamma_b}}{\kappa_m+\Gamma_b+\Gamma_c} \\ \frac{2\sqrt{\Gamma_b\Gamma_c}}{\kappa_m+\Gamma_b+\Gamma_c} & \frac{2i\sqrt{\kappa_m\Gamma_b}}{\kappa_m+\Gamma_b+\Gamma_c} & 0 & i\frac{\kappa_m+\Gamma_c-\Gamma_b}{\kappa_m+\Gamma_b+\Gamma_c} \\ 0 & 0 & i & 0 \end{pmatrix} \tag{14}$$

with $\Gamma_b = 4G_{mb}^2/\kappa_b$ and $\Gamma_c = 4G_{mc}^2/\kappa_c$. It is now clear that the matrix elements $T_{21}(0)$ and $T_{31}(0)$ take the form

$$T_{21}(0) = \frac{2i\sqrt{\kappa_m\Gamma_c}}{\kappa_m+\Gamma_b+\Gamma_c},\ T_{31}(0) = \frac{2\sqrt{\Gamma_b\Gamma_c}}{\kappa_m+\Gamma_b+\Gamma_c}. \tag{15}$$

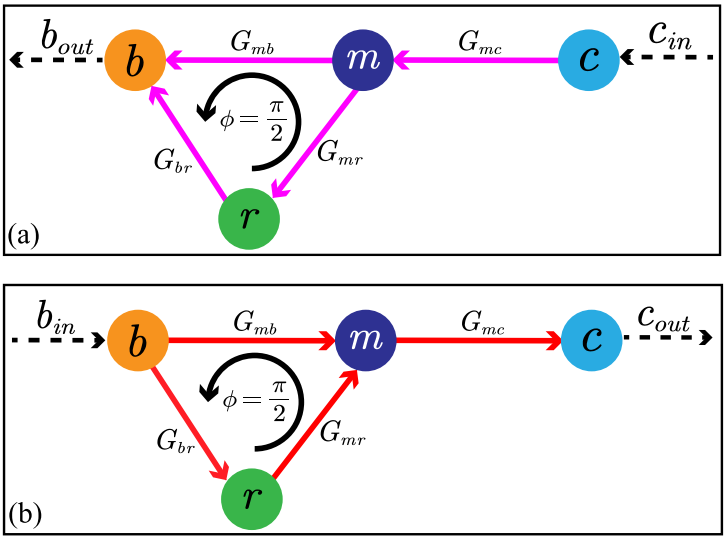

Figure 3. The nonreciprocal conversion between the microwave and optical photons with the synthetic magnetic flux $\phi = \pi/2$. (a) Diagram of the input single-photon state transferred from the microwave mode to the optical mode. (b) Diagram of the input single-photon state transferred from the optical mode to the microwave mode.

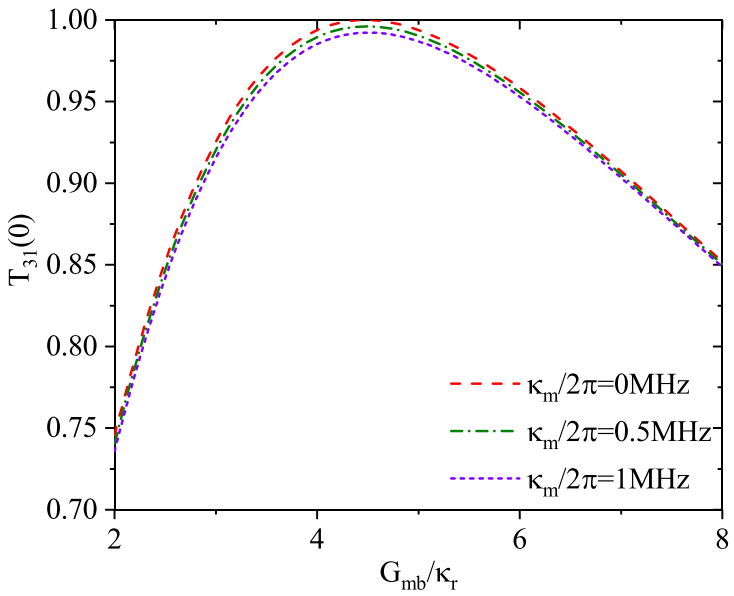

Figure 4. The transmission matrix element $T_{31}(0)$ is plotted vs the dimensionless coupling strength G_{mb}/κ_r under the nonreciprocal conditions. The relevant parameters are chosen as $G_{mc}/\kappa_r = 4$, $\kappa_c/\kappa_r = 2$, $\kappa_b/\kappa_r = 2.5$, and $\kappa_r/2\pi = 2$ MHz.

To highly suppress the state conversion from the microwave mode c to the magnon mode m, we should control the parameters for $\kappa_m \ll \Gamma_b$, such that the condition $|T_{21}(0)/T_{31}(0)| \ll 1$ can be satisfied. If we further set $\Gamma_b \approx \Gamma_c$ (i.e. $G_{mb} \approx G_{mc}\sqrt{\kappa_b/\kappa_c}$), the transmission amplitude $T_{31}(0) \approx 1$ can be achieved. Therefore, by fulfilling the nonreciprocal conditions $|G_{mr}| = G_{mb}\kappa_r/2G_{br}$, $G_{br} = \sqrt{\kappa_b\kappa_r}/2$ and $\phi = \pm\pi/2$, as well as $\kappa_m \ll \Gamma_b \approx \Gamma_c$, we can implement a high-performance nonreciprocal quantum transduction between the optical and microwave modes.

To confirm the above discussion, we plot the transmission matrix element $T_{31}(0) = 2\sqrt{\Gamma_b\Gamma_c}/(\kappa_m + \Gamma_b + \Gamma_c)$ as a function of the coupling constant G_{mb} in figure 4. Under the nonreciprocal conditions, it can be observed that the optimal nonreciprocal single-photon state conversion from the microwave to optical mode (i.e. $T_{31}(0) = 1$ and $T_{13}(0) = 0$) can be realized when $\Gamma_b = \Gamma_c$ and $\kappa_m = 0$. Hence, it proves the validity of our scheme. In a real situation, the dissipation of magnon mode is inevitable to weaken the optical

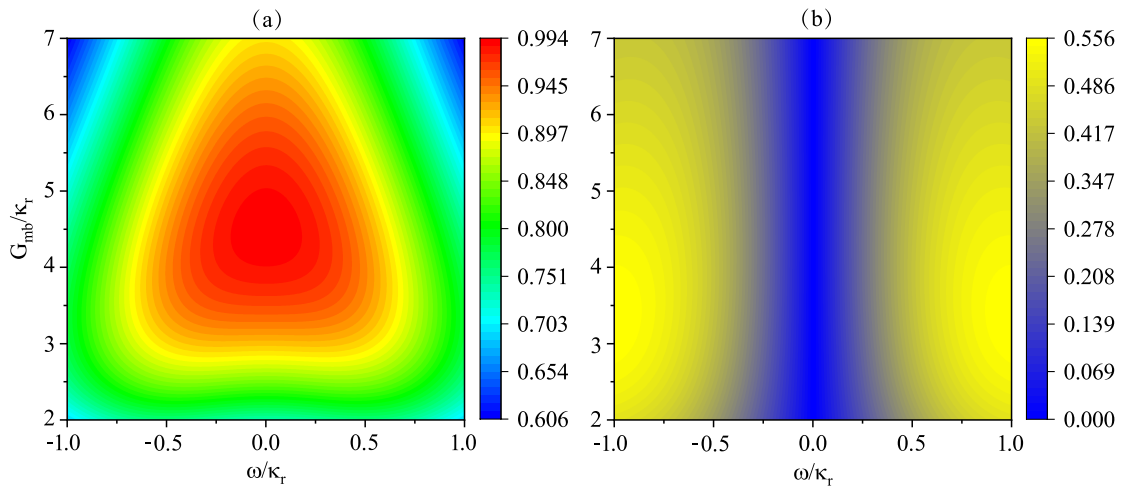

Figure 5. The transmission matrix elements (a) $|T_{31}(\omega)|$ and (b) $|T_{13}(\omega)|$ are plotted as a function of the dimensionless frequency ω/κ_r and coupling strength G_{mb}/κ_r under the nonreciprocal conditions. The other parameters are $G_{mc}/\kappa_r = 4$, $\kappa_c/\kappa_r = 2$, $\kappa_b/\kappa_r = 2.5$, $\kappa_m/\kappa_r = 0.5$ and $\kappa_r/2\pi = 2$ MHz.

nonreciprocity. However, for the most relevant value $\kappa_m/2\pi \approx 1$ MHz in experiments, the condition $\kappa_m \ll \Gamma_b, \Gamma_c$ is well satisfied, which can ensure a high-performance nonreciprocal single-photon state conversion.

In principle, the different frequencies of the input excitations will influence the nonreciprocal conversion. In practice, a microwave (optical) cavity has an internal (intrinsic) decay rate $\kappa_{\rm in} = \omega_0/Q$, where ω_0 is the eigenfrequency and Q is the quality factor. It is obvious that the cavity's intrinsic loss will reduce the conversion fidelity. For a fixed quality factor Q, the different frequencies of input states will suffer from different internal decay rates. From this perspective, the conversion fidelity is frequency-dependent. In our scheme, however, we have considered the microwave (optical) cavity with a high-quality factor, and the associated internal decay rate, which is much smaller than the external one, has been neglected. So, the nonreciprocal conversion has not been affected by the frequencies of the input excitations when the input single-photon is in resonance with the cavity frequency.

Up to now, we have only focused on the nonreciprocal quantum transduction when the input field is in resonance with the cavity frequency, i.e. $\omega = 0$. In practice, the single-photon is typically with a finite bandwidth. In order to investigate the frequency dependence of the optical nonreciprocity, we derive the transmission matrix elements $T_{13}(\omega)$ and $T_{31}(\omega)$ as

$$T_{13}(\omega) = \frac{G_{mc}\sqrt{\kappa_b\kappa_c}(-G_{mb}\gamma_r - G_{br}|G_{mr}|)}{D(\omega)}, \tag{16}$$

$$T_{31}(\omega) = \frac{G_{mc}\sqrt{\kappa_b\kappa_c}(-G_{mb}\gamma_r + G_{br}|G_{mr}|)}{D(\omega)}, \tag{17}$$

where we have $D(\omega) = G_{mc}^2(\gamma_b\gamma_r + G_{br}^2) + \gamma_c(\gamma_m\gamma_b\gamma_r + \gamma_r G_{mb}^2 + \gamma_m G_{br}^2 + \gamma_b|G_{mr}|^2)$, $\gamma_c = i\omega - \kappa_c/2$, $\gamma_m = i\omega - \kappa_m/2$, $\gamma_b = i\omega - \kappa_b/2$ and $\gamma_r = i\omega - \kappa_r/2$. In figure 5, we display the frequency-dependence matrix elements $|T_{31}(\omega)|$ and $|T_{13}(\omega)|$. Based on the chosen parameters in the caption of figure 5, we can see that transmission amplitudes $|T_{31}(\omega)| > 0.99$ and $|T_{13}(\omega)| < 0.1$ can be achieved around the central frequency, which can enable a high-performance nonreciprocal single-photon state conversion from the microwave to optical modes.

Without loss of generality, we consider an input single-photon microwave state that is described as a Gauss wave packet denoted by $|\psi_{c,\rm in}(\omega)\rangle = \int {\rm d}\omega\phi_{\rm in}(\omega)\,|1(\omega)\rangle_c$, where $\phi_{\rm in}(\omega) = [2/(\pi d^2)]^{1/4}e^{-(\omega/d)^2}$ is the normalized spectra amplitude with pulse width d, and $|1(\omega)\rangle_c$ represents the microwave single-photon state of frequency component ω. Since the microwave and optical modes are coupled to the other modes and the environment, the input single-photon microwave state cannot be fully transmitted to the output of the optical mode. As a result, the output optical state is described by

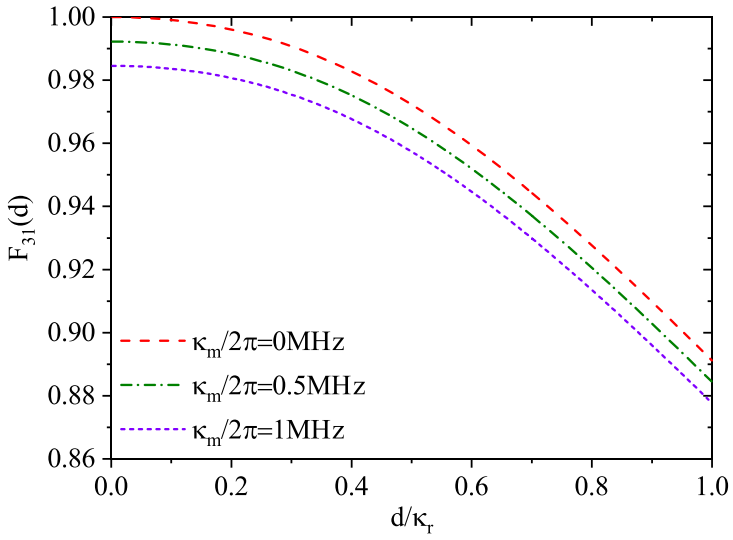

Figure 6. Fidelity $F_{31}(d)$ is plotted as a function of the dimensionless pulse width d/κ_r under the nonreciprocal conditions. The relevant parameters are chosen as $G_{mc}/\kappa_r = 4$, $G_{mb}/\kappa_r = 4.47$, $\kappa_c/\kappa_r = 2$, $\kappa_b/\kappa_r = 2.5$ and $\kappa_r/2\pi = 2$ MHz.

$$\rho_{b,\mathrm{out}} = \int \mathrm{d}\omega[1 - |T_{31}(\omega)\phi_{\mathrm{in}}(\omega)|^2]\,|0(\omega)\rangle_b\langle 0(\omega)| + \int \mathrm{d}\omega\,|T_{31}(\omega)\phi_{\mathrm{in}}(\omega)|^2\,|1(\omega)\rangle_b\langle 1(\omega)|\,. \tag{18}$$

So, the conversion fidelity of the single-photon state is quantified by

$$F_{31}(d) = \int \mathrm{d}\omega\,|T_{31}(\omega)\phi_{\mathrm{in}}(\omega)|^2\,. \tag{19}$$

In our scheme, $|T_{31}(\omega)|$ can be larger than 0.99 around the central frequency, such that most of the microwave single-photon component can be transmitted to the output of optical mode. Figure 6 exhibits the fidelity $F_{31}(d)$ versus the pulse width d of the single-photon state. For $\kappa_m/2\pi = 0.5$ MHz, we can observe that the transmitted fidelity yields $F_{31}(d) \approx 0.97$ for an input microwave single-photon state with the bandwidth $d/2\pi = 1$ MHz. Since the nonreciprocal conversion of a single-photon wave packet with a relatively high fidelity can be achieved between the microwave and optical modes, our scheme may find important applications in long-distance quantum communication and quantum networks.

Finally, it is noted here that our scheme is also applicable to an input signal of weak coherent state. For a weak coherent state $|\alpha\rangle$, α can be treated as a classical number, so that the output state is still a coherent state. In addition, we should emphasize that it is not feasible for an input signal of a strong coherent state. This is because the strong coherent state input can be treated as an additional strong driving for the microwave or optical modes. Then the assumptions for deriving the linearized Hamiltonian (7), as well as the non-reciprocal conditions will be modified. Therefore, our scheme is only available to a weak coherent state input, whose amplitude is much smaller than the steady-state values of microwave or optical modes.

4. Effect of the thermal phonon noise

To investigate the effect of thermal phonon noise to the single-photon state conversion, we introduce the output spectra $S_{b\_\mathrm{out}}(\omega)$ of the cavity mode b, which is defined as $S_{b\_\mathrm{out}}(\omega) = \int_{-\infty}^{\infty} \frac{\mathrm{d}\Omega}{2\pi} \left\langle b_{\mathrm{out}}^{\dagger}(\Omega) b_{\mathrm{out}}(\omega) \right\rangle$. The correlation functions of noise operators in the frequency domain are given by

$$\begin{aligned} &\left\langle c_{\mathrm{in}}^{\dagger}(\Omega) c_{\mathrm{in}}(\omega) \right\rangle = 2\pi S_{c\_\mathrm{in}}(\omega)\delta(\omega+\Omega), \quad \left\langle m_{\mathrm{in}}^{\dagger}(\Omega) m_{\mathrm{in}}(\omega) \right\rangle = 0, \\ &\left\langle b_{\mathrm{in}}^{\dagger}(\Omega) b_{\mathrm{in}}(\omega) \right\rangle = 0, \quad \left\langle r_{\mathrm{in}}^{\dagger}(\Omega) r_{\mathrm{in}}(\omega) \right\rangle = 2\pi\, n_{\mathrm{th}}\delta(\omega+\Omega), \end{aligned} \tag{20}$$

where $S_{c\_\mathrm{in}}(\omega)$ denotes the input spectrum of the microwave mode. Then, the output spectrum of the optical cavity b can be derived as

$$S_{b\_\mathrm{out}}(\omega) = S_{c\_\mathrm{in}}(\omega)\,|T_{31}(\omega)|^2 + n_{\mathrm{th}}\,|T_{34}(\omega)|^2 \tag{21}$$

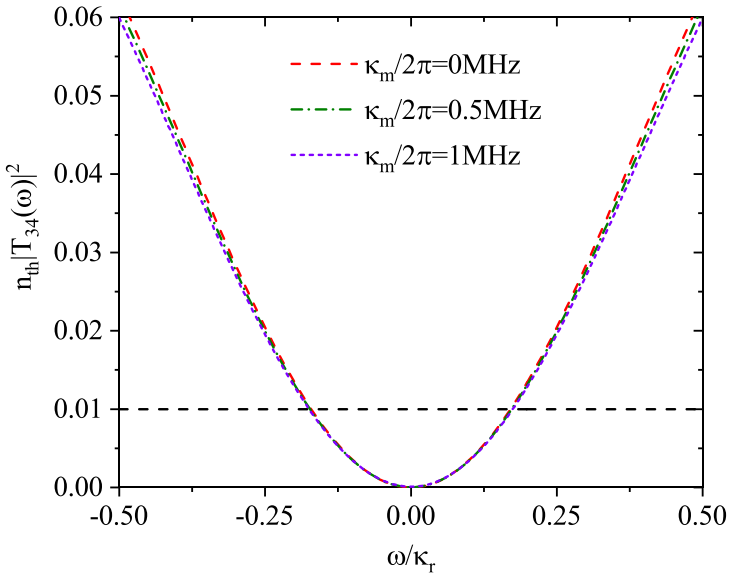

Figure 7. The value $n_{\rm th}\,|T_{34}(\omega)|^2$ is plotted as a function of the frequency ω/κ_r under the nonreciprocal conditions. The relevant parameters are chosen as $n_{\rm th}=1.62$, $G_{mc}/\kappa_r=4$, $G_{mb}/\kappa_r=4.47$, $\kappa_c/\kappa_r=2$, $\kappa_b/\kappa_r=2.5$ and $\kappa_r/2\pi=2$ MHz.

with

$$T_{34}(\omega)=\frac{i\sqrt{\kappa_b\kappa_r}[G_{br}(\gamma_c\gamma_m+G_{mc}^2)+G_{mb}\,|G_{mr}|\,\gamma_c]}{D(\omega)}. \tag{22}$$

The presence of thermal phonon noise will degrade the quality of single-photon state conversion. For the experimental working temperature $T=10$ mK, $n_{\rm th}$ is about 1.62 for a mechanical frequency $\omega_r/2\pi=100$ MHz. To quantitatively describe its effect to the quantum transduction, we exhibit the value $n_{\rm th}\,|T_{34}(\omega)|^2$ as a function of the frequency ω under the nonreciprocal conditions (see figure 7). It is observed that the added thermal excitation is smaller than 0.01 around the central frequency, indicating that the implementation of a high-quality nonreciprocal single-photon state conversion is feasible.

5. Experimental feasibility

Let us now discuss the experimental feasibility of our proposal. To achieve the high-performance of nonreciproccal single-photon state conversion, we have employed the coupling parameters [14, 15, 40, 41, 71, 72]: $G_{mc}/2\pi=8$ MHz, $G_{br}/2\pi=1.58$ MHz, $G_{mr}/2\pi=5.66$ MHz, $G_{mb}/2\pi=8.94$ MHz, $\kappa_b/2\pi=5$ MHz, $\kappa_c/2\pi=4$ MHz, and $\kappa_r/2\pi=2$ MHz. In practical situation, the single excitation coupling rates are typically weak, where the magnomechanical (g_{mr}) [40], optomagnonic (g_m) [71] and optomechanical (g_{br}) [116, 117] interactions are proportional to $1/D^2$, $1/\sqrt{D^3}$ and $1/D$, respectively, i.e. D is the diameter of a YIG sphere. For a magnetic sphere with $D\sim 30$ μm, the single excitation coupling rates are calculated as $g_{mr}=20$ Hz, $g_m=100$ Hz and $g_{br}=50$ Hz. Therefore, to obtain the desired couplings, the strong external driving fields are needed with driving powers $P_a=98.8$ mW, $P_b=34.2$ mW, and $P_m=4.6$ mW. Up to now, most experiments have mainly exploited the submillimeter diameter YIG sphere. And the one with a 30 μm diameter hasn't been reported in experiment. Considering the 36 μm diameter Silica microsphere [116] having already been demonstrated in experiment, the YIG sphere about 30 μm diameter is expected to be experimentally realized with the rapid development of magnonic systems. In addition, the smaller size of YIG sphere (i.e. 1 μm diameter or even smaller) has already been studied theoretically for the generation of magnonic cat states [79, 118] and frequency conversion between microwave and optical photons [90]. Therefore, we believe that our work will be instructive to the future experiments.

On the other hand, the single excitation coupling rates (g_{mr}, g_m, g_{br}) can be further enhanced by engineering the optomagnonic cavity structure such as microrings to increase the mode overlap [72, 84, 90, 117, 119]. Especially, single-photon coupling rate g_m can be increased by purifying and doping YIG [120], and utilizing the epsilon-near-zero medium [88]. With the rapid development in cavity magnomechanics and optomagnonics, we believe our scheme is expected to be realized in the future experiments.

6. Summary

In summary, we have put forward an efficient scheme to realize the nonreciprocal single-photon state conversion between the microwave and optical domains based on a hybrid magnonic system, in which a YIG sphere with both the optomechanical and optomagnetic properties is coupled to a three-dimensional microwave cavity. The magnetostatic mode as a mediator is coupled to the microwave and optical modes simultaneously. By controlling the magnitude ratios and phase differences of the couplings via external driving fields, we can acquire a relatively high-fidelity nonreciprocal microwave-light single-photon state conversion via the quantum interference effect. Our work provides an appealing way for implementing unidirectional quantum transduction between the microwave and optical photons, which is vital for long-distance quantum networks and distributed quantum information processing.

Data availability statement

The data cannot be made publicly available upon publication because they are not available in a format that is sufficiently accessible or reusable by other researchers. The data that support the findings of this study are available upon reasonable request from the authors.

Acknowledgments

This work was supported by the National Natural Science Foundation of China (Grant Nos. 12074307 and 11704306), the Fundamental Research Funds for the Central Universities (Grant No. 11913291000022), and the Doctoral Scientific Research Foundation of Hubei University of Automotive Technology (Grant No. BK202113).

Conflict of interest

The authors declare no conflict of interest.

Appendix. Derivation of the effective linearized Hamiltonian

In this appendix, we give a detailed derivation of the effective linearized Hamiltonian in equation (6) with the key approximations. Substituting the Hamiltonian of equation (5) into the Heisenberg equation $\mathrm{d}A/\mathrm{d}t = i[H_t, A]$ and taking into account the damping terms, we can get the quantum Langevin equations (QLEs)

$$\frac{\mathrm{d}a}{\mathrm{d}t} = -\left(i\Delta_a' + \frac{\kappa_a}{2}\right)a - ig_m bm^\dagger - i\Omega_a e^{-i\theta_m}, \tag{A.1}$$

$$\frac{\mathrm{d}b}{\mathrm{d}t} = -\left(i\Delta_b' + \frac{\kappa_b}{2}\right)b - ig_m am - ig_{br}b\left(r^\dagger + r\right) - i\Omega_b e^{-i\theta_b}, \tag{A.2}$$

$$\frac{\mathrm{d}c}{\mathrm{d}t} = -\left(i\Delta_c' + \frac{\kappa_c}{2}\right)c - iG_{mc}m, \tag{A.3}$$

$$\begin{aligned}\frac{\mathrm{d}m}{\mathrm{d}t} = &-\left(i\Delta_m' + \frac{\kappa_m}{2}\right)m - ig_m a^\dagger b - iG_{mc}c \\ &- ig_{mr}m\left(r^\dagger + r\right) - i\Omega_m e^{-i\theta_m},\end{aligned} \tag{A.4}$$

$$\frac{\mathrm{d}r}{\mathrm{d}t} = -\left(i\omega_r + \frac{\kappa_r}{2}\right)r - ig_{br}b^\dagger b - ig_{mr}m^\dagger m, \tag{A.5}$$

where κ_α, κ_r describe the decay rate ($\alpha = a, b, c, m$). When the driving fields are strong enough, the operators can be rewritten as the sum of a classical mean value and a small quantum fluctuation operator, i.e. $\alpha = \alpha_s + \delta\alpha$ and $r = r_s + \delta r$. Taking them into equations (A.1)–(A.5), we can first obtain the steady-state values of α_s and r_s

$$0 = -\left(i\Delta_a + \frac{\kappa_a}{2}\right) a_s - ig_m b_s m_s^* - i\Omega_a e^{-i\theta_a}, \tag{A.6}$$

$$0 = -\left(i\Delta_b + \frac{\kappa_b}{2}\right) b_s - iG_{mb} m_s - i\Omega_b e^{-i\theta_b}, \tag{A.7}$$

$$0 = -\left(i\Delta_c + \frac{\kappa_c}{2}\right) c_s - iG_{mc} m_s, \tag{A.8}$$

$$0 = -\left(i\Delta_m + \frac{\kappa_m}{2}\right) m_s - iG_{mb}^* b_s - iG_{mc} c_s - i\Omega_m e^{-i\theta_m}, \tag{A.9}$$

$$0 = -\left(i\omega_r + \frac{\kappa_r}{2}\right) r_s - ig_{br} |b_s|^2 - ig_{mr} |m_s|^2 \tag{A.10}$$

with $\Delta_a = \Delta_a'$, $\Delta_b = \Delta_b' + g_{br}(r_s^* + r_s)$, $\Delta_c = \Delta_c'$ and $\Delta_m = \Delta_m^{'} + g_{mr}(r_s^* + r_s)$.

For $|\alpha_s| \gg 1$ and $|r_s| \gg 1$, we can discard those nonlinear terms and derive the linearized QLEs of the quantum fluctuation operators

$$\frac{\mathrm{d}\delta a}{\mathrm{d}t} = -\left(i\Delta_a + \frac{\kappa_a}{2}\right) \delta a - i\left(G_{am}\delta m^\dagger + G_{ab}^*\delta b\right), \tag{A.11}$$

$$\frac{\mathrm{d}\delta b}{\mathrm{d}t} = -\left(i\Delta_b + \frac{\kappa_b}{2}\right) \delta b - i\left(G_{mb}\delta m + G_{ab}\delta a\right) - iG_{br}\left(\delta r^\dagger + \delta r\right), \tag{A.12}$$

$$\frac{\mathrm{d}\delta c}{\mathrm{d}t} = -\left(i\Delta_c + \frac{\kappa_c}{2}\right) \delta c - iG_{mc}\delta m, \tag{A.13}$$

$$\begin{aligned}\frac{\mathrm{d}\delta m}{\mathrm{d}t} = &-\left(i\Delta_m + \frac{\kappa_m}{2}\right) \delta m - i\left(G_{mb}^*\delta b + G_{am}\delta a^\dagger\right) \\ &- iG_{mc}\delta c - iG_{mr}^*\left(\delta r^\dagger + \delta r\right),\end{aligned} \tag{A.14}$$

$$\begin{aligned}\frac{\mathrm{d}\delta r}{\mathrm{d}t} = &-\left(i\omega_r + \frac{\kappa_r}{2}\right) \delta r - i\left(G_{br}^*\delta b + G_{br}\delta b^\dagger\right) \\ &- i\left(G_{mr}\delta m + G_{mr}^*\delta m^\dagger\right)\end{aligned} \tag{A.15}$$

with the field-enhanced coupling strengths $G_{am} = g_m b_s$, $G_{ab} = g_m m_s$, $G_{mb} = g_m a_s$, $G_{br} = g_{br} b_s$ and $G_{mr} = g_{mr} m_s^*$. Then, we can figure out the effective linearized Hamiltonian

$$\begin{aligned}H_{lin} = &\sum_\alpha \Delta_\alpha \alpha^\dagger \alpha + \omega_r r^\dagger r + \left[G_{ab} a b^\dagger + G_{am} a^\dagger m^\dagger + G_{mc} m c^\dagger + G_{mb} m b^\dagger\right. \\ &\left. + \left(G_{br} b^\dagger + G_{mr} m\right)\left(r^\dagger + r\right) + H.c.\right],\end{aligned} \tag{A.16}$$

where we have redefined $\delta\alpha \longrightarrow \alpha$ and $\delta r \longrightarrow r$. It is just the Hamiltonian in equation (6) of the main text.

ORCID iDs

Yalong Ren https://orcid.org/0000-0002-8049-1895
Xinke Li https://orcid.org/0000-0001-6533-9388

References

[1] Wallquist M, Hammerer K, Rabl P, Lukin M and Zoller P 2009 *Phys. Scr.* **T137** 014001
[2] Kurizki G, Bertet P, Kubo Y, Mølmer K, Petrosyan D, Rabl P and Schmiedmayer J 2015 *Proc. Natl Acad. Sci.* **112** 3866–73
[3] Xiang Z L, Ashhab S, You J Q and Nori F 2013 *Rev. Mod. Phys.* **85** 623–53
[4] Forn-Díaz P, García-Ripoll J J, Peropadre B, Orgiazzi J L, Yurtalan M A, Belyansky R, Wilson C M and Lupascu A 2016 *Nat. Phys.* **13** 39–43
[5] Kandala A, Mezzacapo A, Temme K, Takita M, Brink M, Chow J M and Gambetta J M 2017 *Nature* **549** 242–6
[6] Huebl H, Zollitsch C W, Lotze J, Hocke F, Greifenstein M, Marx A, Gross R and Goennenwein S T B 2013 *Phys. Rev. Lett.* **111** 127003
[7] Hou J T and Liu L 2019 *Phys. Rev. Lett.* **123** 107702
[8] Li Y *et al* 2019 *Phys. Rev. Lett.* **123** 107701
[9] Lachance-Quirion D, Tabuchi Y, Gloppe A, Usami K and Nakamura Y 2019 *Appl. Phys. Express* **12** 070101
[10] Rameshti B Z, Kusminskiy S V, Haigh J A, Usami K, Lachance-Quirion D, Nakamura Y, Hu C M, Tang H X, Bauer G E and Blanter Y M 2022 *Phys. Rep.* **979** 1–61

[11] Yuan H, Cao Y, Kamra A, Duine R A and Yan P 2022 *Phys. Rep.* **965** 1–74
[12] Clerk A A, Lehnert K W, Bertet P, Petta J R and Nakamura Y 2020 *Nat. Phys.* **16** 257–67
[13] Zare Rameshti B and Bauer G E W 2018 *Phys. Rev.* B **97** 014419
[14] Tabuchi Y, Ishino S, Ishikawa T, Yamazaki R, Usami K and Nakamura Y 2014 *Phys. Rev. Lett.* **113** 083603
[15] Zhang X, Zou C L, Jiang L and Tang H X 2014 *Phys. Rev. Lett.* **113** 156401
[16] Lambert N J, Haigh J A, Langenfeld S, Doherty A C and Ferguson A J 2016 *Phys. Rev.* A **93** 021803
[17] Li Y *et al* 2022 *Phys. Rev. Lett.* **128** 047701
[18] Yang Y, Rao J, Gui Y, Yao B, Lu W and Hu C M 2019 *Phys. Rev. Appl.* **11** 054023
[19] Boventer I, Dörflinger C, Wolz T, Macêdo R, Lebrun R, Kläui M and Weides M 2020 *Phys. Rev. Res.* **2** 013154
[20] Zhang D, Wang X M, Li T F, Luo X Q, Wu W, Nori F and You J 2015 *npj Quantum Inf.* **1** 15014
[21] Kostylev N, Goryachev M and Tobar M E 2016 *Appl. Phys. Lett.* **108** 062402
[22] Goryachev M, Farr W G, Creedon D L, Fan Y, Kostylev M and Tobar M E 2014 *Phys. Rev. Appl.* **2** 054002
[23] Wang Y P, Zhang G Q, Zhang D, Li T F, Hu C M and You J 2018 *Phys. Rev. Lett.* **120** 057202
[24] Wang Y P, Zhang G Q, Zhang D, Luo X Q, Xiong W, Wang S P, Li T F, Hu C M and You J Q 2016 *Phys. Rev.* B **94** 224410
[25] Zhang X, Zou C L, Zhu N, Marquardt F, Jiang L and Tang H X 2015 *Nat. Commun.* **6** 8914
[26] Bi M X, Yan X H, Xiao Y and Dai C J 2020 *J. Appl. Phys.* **127** 223909
[27] Lachance-Quirion D, Tabuchi Y, Ishino S, Noguchi A, Ishikawa T, Yamazaki R and Nakamura Y 2017 *Sci. Adv.* **3** e1603150
[28] Grigoryan V L and Xia K 2020 *Phys. Rev.* B **102** 064426
[29] Lachance-Quirion D, Wolski S P, Tabuchi Y, Kono S, Usami K and Nakamura Y 2020 *Science* **367** 425–8
[30] Wolski S, Lachance-Quirion D, Tabuchi Y, Kono S, Noguchi A, Usami K and Nakamura Y 2020 *Phys. Rev. Lett.* **125** 117701
[31] Crescini N, Braggio C, Carugno G, Ortolan A and Ruoso G 2020 *Appl. Phys. Lett.* **117** 144001
[32] Wang Y P, Rao J, Yang Y, Xu P C, Gui Y, Yao B, You J and Hu C M 2019 *Phys. Rev. Lett.* **123** 127202
[33] Zhao Y, Rao J, Gui Y, Wang Y and Hu C M 2020 *Phys. Rev. Appl.* **14** 014035
[34] Zhang X, Ding K, Zhou X, Xu J and Jin D 2019 *Phys. Rev. Lett.* **123** 237202
[35] Zhang D, Luo X Q, Wang Y P, Li T F and You J Q 2017 *Nat. Commun.* **8** 1368
[36] Xu J, Zhong C, Han X, Jin D, Jiang L and Zhang X 2020 *Phys. Rev. Lett.* **125** 237201
[37] Xu P C, Rao J W, Gui Y S, Jin X and Hu C M 2019 *Phys. Rev.* B **100** 094415
[38] Crescini N, Braggio C, Carugno G, Ortolan A and Ruoso G 2021 *Phys. Rev.* B **104** 064426
[39] Rao J W, Yu C H, Zhao Y T, Gui Y S, Fan X L, Xue D S and Hu C M 2019 *New J. Phys.* **21** 065001
[40] Zhang X, Zou C L, Jiang L and Tang H X 2016 *Sci. Adv.* **2** e1501286
[41] Potts C, Varga E, Bittencourt V, Kusminskiy S V and Davis J 2021 *Phys. Rev.* X **11** 031053
[42] Li J, Zhu S Y and Agarwal G 2018 *Phys. Rev. Lett.* **121** 203601
[43] Zhang Z, Scully M O and Agarwal G S 2019 *Phys. Rev. Res.* **1** 023021
[44] Li J and Zhu S Y 2019 *New J. Phys.* **21** 085001
[45] Yu M, Shen H and Li J 2020 *Phys. Rev. Lett.* **124** 213604
[46] Luo D W, Qian X F and Yu T 2021 *Opt. Lett.* **46** 1073
[47] Yuan H, Yan P, Zheng S, He Q, Xia K and Yung M H 2020 *Phys. Rev. Lett.* **124** 053602
[48] Yang Z B, Jin H, Jin J W, Liu J Y, Liu H Y and Yang R C 2021 *Phys. Rev. Res.* **3** 023126
[49] Nair J M P and Agarwal G S 2020 *Appl. Phys. Lett.* **117** 084001
[50] Li J and Gröblacher S 2021 *Quantum Sci. Technol.* **6** 024005
[51] Nair J M, Mukhopadhyay D and Agarwal G 2021 *Phys. Rev. Lett.* **126** 180401
[52] Zhang G Q and You J Q 2019 *Phys. Rev.* B **99** 054404
[53] Lu T X, Zhang H, Zhang Q and Jing H 2021 *Phys. Rev.* A **103** 063708
[54] Grigoryan V L and Xia K 2022 *Phys. Rev.* B **106** 014404
[55] Boventer I, Kläui M, Macêdo R and Weides M 2019 *New J. Phys.* **21** 125001
[56] Ding M S, Zheng L and Li C 2019 *Sci. Rep.* **9** 15723
[57] Xu Y, Liu J Y, Liu W and Xiao Y F 2021 *Phys. Rev.* A **103** 053501
[58] Kun Xie J, Li Ma S and Li F L 2020 *Phys. Rev.* A **101** 042331
[59] Liu Z X, Xiong H and Wu Y 2019 *Phys. Rev.* B **100** 134421
[60] Zhao C, Li X, Chao S, Peng R, Li C and Zhou L 2020 *Phys. Rev.* A **101** 063838
[61] Yuan H Y and Duine R A 2020 *Phys. Rev.* B **102** 100402
[62] Wu K, Xue Zhong W, Ling Cheng G and Xi Chen A 2021 *Phys. Rev.* A **103** 052411
[63] Kong C, Xiong H and Wu Y 2019 *Phys. Rev. Appl.* **12** 034001
[64] Zhu N, Han X, Zou C L, Xu M and Tang H X 2020 *Phys. Rev.* A **101** 043842
[65] Yu W, Yu T and Bauer G E W 2020 *Phys. Rev.* B **102** 064416
[66] Long Ren Y, Li Ma S, Kun Xie J, Ke Li X, Tao Cao M and Li Li F 2022 *Phys. Rev.* A **105** 013711
[67] Haigh J A, Langenfeld S, Lambert N J, Baumberg J J, Ramsay A J, Nunnenkamp A and Ferguson A J 2015 *Phys. Rev.* A **92** 063845
[68] Sharma S, Blanter Y M and Bauer G E W 2017 *Phys. Rev.* B **96** 094412
[69] Osada A, Gloppe A, Nakamura Y and Usami K 2018 *New J. Phys.* **20** 103018
[70] Haigh J A, Lambert N J, Sharma S, Blanter Y M, Bauer G E W and Ramsay A J 2018 *Phys. Rev.* B **97** 214423
[71] Osada A, Hisatomi R, Noguchi A, Tabuchi Y, Yamazaki R, Usami K, Sadgrove M, Yalla R, Nomura M and Nakamura Y 2016 *Phys. Rev. Lett.* **116** 223601
[72] Zhang X, Zhu N, Zou C L and Tang H X 2016 *Phys. Rev. Lett.* **117** 123605
[73] Osada A, Gloppe A, Hisatomi R, Noguchi A, Yamazaki R, Nomura M, Nakamura Y and Usami K 2018 *Phys. Rev. Lett.* **120** 133602
[74] Hisatomi R, Noguchi A, Yamazaki R, Nakata Y, Gloppe A, Nakamura Y and Usami K 2019 *Phys. Rev. Lett.* **123** 207401
[75] Haigh J, Nunnenkamp A, Ramsay A and Ferguson A 2016 *Phys. Rev. Lett.* **117** 133602
[76] Bittencourt V A S V, Feulner V and Kusminskiy S V 2019 *Phys. Rev.* A **100** 013810
[77] Liu Z X and Xiong H 2020 *Opt. Lett.* **45** 5452
[78] Sharma S, Blanter Y M and Bauer G E 2018 *Phys. Rev. Lett.* **121** 087205
[79] Sun F X, Zheng S S, Xiao Y, Gong Q, He Q and Xia K 2021 *Phys. Rev. Lett.* **127** 087203
[80] Gao Y P, Cao C, Duan Y W, Liu X F, Pang T T, Wang T J and Wang C 2019 *Nanophotonics* **9** 1953–61
[81] Gao Y P, Cao C, Wang T J, Zhang Y and Wang C 2017 *Phys. Rev.* A **96** 023826
[82] Xie H, Shi Z G, He L W, Chen X, Liao C G and Lin X M 2022 *Phys. Rev.* A **105** 023701

[83] Wang B, Jia X, Lu X H and Xiong H 2022 *Phys. Rev.* A **105** 053705
[84] Liu T, Zhang X, Tang H X and Flatté M E 2016 *Phys. Rev.* B **94** 060405
[85] Wu W J, Wang Y P, Wu J Z, Li J and You J Q 2021 *Phys. Rev.* A **104** 023711
[86] Gao Y P, Liu X F, Wang T J, Cao C and Wang C 2019 *Phys. Rev.* A **100** 043831
[87] Li J, Wang Y P, Wu W J, Zhu S Y and You J 2021 *PRX Quantum* **2** 040344
[88] Bittencourt V A S V, Liberal I and Viola Kusminskiy S 2022 *Phys. Rev. Lett.* **128** 183603
[89] Cai Q, Liao J and Zhou Q 2020 *Ann. Phys., Lpz.* **532** 2000250
[90] Engelhardt F, Bittencourt V, Huebl H, Klein O and Kusminskiy S V 2022 *Phys. Rev. Appl.* **18** 044059
[91] Mukhopadhyay D, Nair J M P and Agarwal G S 2022 *Phys. Rev.* B **105** 064405
[92] Hisatomi R, Osada A, Tabuchi Y, Ishikawa T, Noguchi A, Yamazaki R, Usami K and Nakamura Y 2016 *Phys. Rev.* B **93** 174427
[93] Ihn Y S, Lee S Y, Kim D, Yim S H and Kim Z 2020 *Phys. Rev.* B **102** 064418
[94] Chai C Z, Shen Z, Zhang Y L, Zhao H Q, Guo G C, Zou C L and Dong C H 2022 *Photon. Res.* **10** 820
[95] Han X, Fu W, Zou C L, Jiang L and Tang H X 2021 *Optica* **8** 1050
[96] Wang Y D and Clerk A A 2012 *Phys. Rev. Lett.* **108** 153603
[97] Tian L 2012 *Phys. Rev. Lett.* **108** 153604
[98] Bochmann J, Vainsencher A, Awschalom D D and Cleland A N 2013 *Nat. Phys.* **9** 712–6
[99] Bagci T *et al* 2014 *Nature* **507** 81–85
[100] Andrews R W, Peterson R W, Purdy T P, Cicak K, Simmonds R W, Regal C A and Lehnert K W 2014 *Nat. Phys.* **10** 321–6
[101] Petrosyan D, Mølmer K, Fortágh J and Saffman M 2019 *New J. Phys.* **21** 073033
[102] Metelmann A and Clerk A 2015 *Phys. Rev.* X **5** 021025
[103] Fang K, Luo J, Metelmann A, Matheny M H, Marquardt F, Clerk A A and Painter O 2017 *Nat. Phys.* **13** 465–71
[104] Xu X W, Li Y, Chen A X and Liu Y X 2016 *Phys. Rev.* A **93** 023827
[105] Tian L and Li Z 2017 *Phys. Rev.* A **96** 013808
[106] Jiang C, Song L N and Li Y 2019 *Phys. Rev.* A **99** 023823
[107] Eshaqi-Sani N, Zippilli S and Vitali D 2022 *Phys. Rev.* A **106** 032606
[108] Kittel C 1948 *Phys. Rev.* **73** 155–61
[109] Tzuang L D, Fang K, Nussenzveig P, Fan S and Lipson M 2014 *Nat. Photon.* **8** 701–5
[110] Estep N A, Sounas D L, Soric J and Alù A 2014 *Nat. Phys.* **10** 923–7
[111] Koch J, Houck A A, Hur K L and Girvin S M 2010 *Phys. Rev.* A **82** 043811
[112] Nunnenkamp A, Koch J and Girvin S M 2011 *New J. Phys.* **13** 095008
[113] Roy D, Wilson C and Firstenberg O 2017 *Rev. Mod. Phys.* **89** 021001
[114] Fleury R, Sounas D L, Sieck C F, Haberman M R and Alù A 2014 *Science* **343** 516–9
[115] Xu X W and Li Y 2015 *Phys. Rev.* A **91** 053854
[116] Shen Z, Zhang Y L, Chen Y, Zou C L, Xiao Y F, Zou X B, Sun F W, Guo G C and Dong C H 2016 *Nat. Photon.* **10** 657–61
[117] Aspelmeyer M, Kippenberg T J and Marquardt F 2014 *Rev. Mod. Phys.* **86** 1391–452
[118] Kounalakis M, Bauer G E and Blanter Y M 2022 *Phys. Rev. Lett.* **129** 037205
[119] Wu X Y, Zhang Y, Gao Y P and Wang C 2021 *Opt. Express* **29** 40061
[120] Almpanis E 2018 *Phys. Rev.* B **97** 184406